

Dynamics of particle sedimentation in a vertical channel: Period-doubling bifurcation and chaotic state^{a)}

Cyrus K. Aidun^{b)} and E-Jiang Ding

G. W. Woodruff School of Mechanical Engineering and Institute of Paper Science and Technology, Georgia Institute of Technology, 500 10th Street, N.W. Atlanta, Georgia 30318

(Received 11 June 2002; accepted 27 February 2003; published 5 May 2003)

The dynamics and interaction of two circular cylinders settling in an infinitely long narrow channel (width equal to four times the cylinder diameter) is explained by direct computational analysis. The results show that at relatively low Reynolds numbers (based on the average particle velocity and diameter), the particles undergo complex transitions to reach a low-dimensional chaotic state represented by a strange attractor. As the Reynolds number increases, the initial periodic state goes through a turning point and a subcritical transition to another periodic branch. Further increase in the Reynolds number results in a cascade of period-doubling bifurcations to a chaotic state represented by a low dimensional chaotic attractor. The entire sequence of transitions takes place in a relatively narrow range of Reynolds number between 2 and 6. The physical reason for the period-doubling transitions is explained based on the interaction of the particles with each other and the channel walls. The particles undergo near contact interactions as settling in the channel. To accurately capture the dynamics, the computational method requires accurate resolution of the particle interactions. The computational results are obtained with our lattice-Boltzmann method developed for suspended particles near contact. The results show that even in the most simple and ideal multiparticle sedimentation, the system undergoes transition to complex dynamics at relatively low Reynolds number. © 2003 American Institute of Physics. [DOI: 10.1063/1.1571825]

I. INTRODUCTION

It is well known that interaction of particles suspended in fluid plays an important role in particle dynamics. At zero and low Reynolds number limits, this problem has been investigated extensively,^{1–4} including sedimentation in the Stokes regime. For small but finite Reynolds number, perturbation methods are used to determine the weak effects of inertia.^{5–7} However, when the Reynolds number is not small, the nonlinear effects of the fluid inertia and the solid particle inertia on the flow are not well understood. Direct computational methods have been demonstrated to be effective in investigating this complex problem.^{8–14}

It has been shown that the basic mechanisms that control the motion and interactions of spherical objects sedimenting in a vertical channel are associated with wakes and turning couples.¹⁵ The sedimentation of circular cylinders considered in this study is also investigated by Hu, Joseph, and Crochet⁸ and Feng, Hu, and Joseph,¹⁵ from now on referred to as Joseph *et al.* Through experiments and direct numerical simulations, Joseph *et al.* have found the trajectory of the particles at low and high Reynolds numbers (Re) with damped oscillation at low Re and an irregular unsteady motion, they termed “drafting-kissing-tumbling” at high Re. The dynamical characteristics of this system, as Re increases

from zero, has not been explored in the past. To gain better fundamental understanding of particle sedimentation, we investigate the particle and flow behavior as the Reynolds number increases.

We use the lattice-Boltzmann method for the direct analysis of solid particles suspended in fluid.^{16–22} By combining Newtonian dynamics of the solid particles with a lattice-Boltzmann model of the fluid, the motion of the particles and the flow field can be simulated efficiently and accurately. An advantage of the lattice-Boltzmann method is that the numerical operations can be easily distributed over parallel processors due to the local nature of the time evolution operator. The result presented in the following sections is based on the ALD²² method, which is the same as the ALD²⁰ method with the addition of virtual boundary nodes to accurately capture the lubrication forces when the particle separation is smaller than a lattice length unit. This method will allow accurate capture of the physics of the particles near contact without the need to use an excessively large grid system.

The outline of the problem and the parameters in the physical and computational space are provided in Sec. II. The initial transition from steady state to periodic state and the transition route to a low-dimensional chaotic state are outlined in the following sections with the last section focusing on the discussion and conclusions.

II. THE PROBLEM DESCRIPTION

In this study, the motion and interaction of two particles during sedimentation in a two-dimensional channel is con-

^{a)}This paper was originally presented as part of the Dan Joseph Symposium on Multi-Component and Multiphase Fluid Dynamics, in conjunction with the 14th U.S. National Congress of Applied Mechanics at Virginia Tech., Blacksburg, VA, 24–28 June 2002.

^{b)}Author to whom correspondence should be addressed.

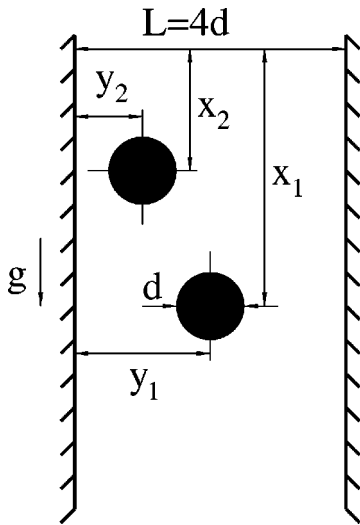


FIG. 1. Problem description and notations used in the calculation of the motion and interaction between two solid particles setting in a channel.

sidered. Two circular cylinders of diameter d and particle–fluid density ratio $\alpha = \rho_p / \rho_f = 1.002$ (ρ_p and ρ_f are the particle and fluid density, respectively) are released in a vertical channel of width $L = 4d$ to settle under a constant force, such as gravity, as shown in Fig. 1. Two types of initial conditions are used in this study. In the first type the particles are released in the vertical channel with zero initial velocity. The initial position of the particles is midway between the centerline of the channel and the sidewall, while one particle is $2d$ above the other. In other words, at $t = 0$, the particles are located at $y_1 = y_2 = d$ and $\delta x = x_1 - x_2 = 2d$. The second type of initial condition and the reasons for it will be discussed in Sec. IV.

The particle Reynolds number is defined as

$$\text{Re} = \frac{Ud}{\nu}, \quad (1)$$

and the Froude number is defined as

$$\text{Fr} = \frac{U^2}{gd}, \quad (2)$$

where ν is the kinematic viscosity, g is gravity, and U is the average terminal velocity (at equilibrium state) of the leading particle. The terminology “equilibrium state” is used in this paper in the context of dynamical systems where the initial transients are passed and the system has reached a stable attractor. The ratio $G \equiv \text{Re}^2 / \text{Fr}$ is then independent of the velocity U , that is

$$G = \frac{\text{Re}^2}{\text{Fr}} = \frac{d^3 g}{\nu^2}. \quad (3)$$

Computational results using a finite element method to solve the continuum equation for the system are given by Joseph *et al.* at $\text{Re} = 100$,⁸ and at $\text{Re} = 2.87$.¹⁵ Their simulations show that at $\text{Re} = 100$ the trailing particle approaches the leading one; jointly, the particles enter into a damped oscillation without contacting each other. On the other hand, at $\text{Re} = 2.87$ the particles reach steady state through damped

oscillation of the initial transients. This system represents a simple and ideal sedimentation process in a confined channel. It is, therefore, important to understand the mechanism of transition to unsteady state as the Reynolds number increases. Because particles repeatedly come into near contact with each other during the sedimentation, this problem is also an ideal candidate for application and evaluation of the ALD’ lattice-Boltzmann method.²²

In order to explore the dynamics and the physics of this two-particle sedimentation system, the particle behavior in the range of Reynolds numbers from 2 to 6 has been explored. With the advantages of the computational method presented in Ref. 22, a relatively small number of lattice nodes are needed in these simulations. The typical size of the computational domain is $d = 32$ and $L \times H = 128 \times 800$ lattice units. The infinitely long channel is simulated with the finite computational domain moving with sufficiently long sections of the fluid channel upstream and downstream of the particles.²⁰ The leading particle is always $10d$ from the bottom of the computational domain where zero velocity is applied uniformly. The top of the computational domain, where the stress-free boundary condition is applied, is always $15d$ downstream of the leading particle.

The particles are driven by external force, f_e , which may include gravity and any other force on the particle in the vertical direction. If only gravity is included, for a circular cylinder in a vertical channel, the net external force (per unit length) is

$$f_e = \frac{\pi}{4} d^2 (\rho_p - \rho_f) g. \quad (4)$$

The dimensionless force, F , is defined as

$$F = f_e d / \rho_f \nu^2. \quad (5)$$

From Eqs. (3)–(5) the external force, written as

$$F = \frac{\pi}{4} G (\alpha - 1) \quad (6)$$

can also be thought of as gravity based Reynolds number.

In order to explain the procedure for setting up a physical problem in the lattice-Boltzmann simulations, let us consider a physical system where the viscosity of fluid is $\nu_s = 0.01 \text{ cm}^2/\text{s}$, the diameter of the circular cylinder is $d_s = 0.2 \text{ cm}$, gravity is $g_s = 980 \text{ cm/s}^2$, and the density ratio is $\alpha = 1.002$. Variables based on the physical quantities are defined by subscript, s . The ratio G for this system can be obtained from Eq. (3) to be $G = 78400$. Hence the dimensionless external force, from Eq. (6), is $F = 123.15$.

In lattice-Boltzmann simulation we set $d = 32$ lattice units, $\rho_f = 1.0$, $\alpha = 1.002$, and $\nu = 1/4$. Then considering that the value of F , being the nondimensional parameter in the problem, should be the same in the continuum and the lattice-Boltzmann systems, from Eq. (5) we find that the external force in the lattice-Boltzmann scale for simulating this physical system should be

$$f_e = \frac{F \rho_f \nu^2}{d} = \frac{123.15 \times 1.0 \times 1/16}{32} \approx 0.24.$$

This example is provided to demonstrate the scaling between the dimensional and the numerical variables. The key is that the dimensionless parameter, in this case the force or the gravity-based Reynolds number, must remain the same.

III. TRANSITION FROM PRIMARY BASE STATE TO PERIODIC STATE THROUGH HOPF BIFURCATION

For dimensionless force $F=131.41$, corresponding to the particle Reynolds number $Re=2.539$, the motion of the particles are represented in Fig. 2. As stated earlier, the length and time are scaled by d and d^2/ν , respectively. Once released from rest, the two particles draft to the right wall as they settle inside the channel. The leading particle then falls along the right wall, while the trailing particle drafts back to the left wall and then the particles enter a damped oscillation. This result is similar to that obtained in previous studies at $Re=2.87$.¹⁵ In this study we fix the density ratio, such that $\alpha=1.002$, while in Ref. 15 the target Reynolds number is obtained by varying the density of the solid particle. Since the value for the density ratio at Reynolds number $Re=2.87$ used for calculation in Ref. 15 is not available, a direct quantitative comparison is not possible.

Starting from rest at $F=131.41$, the two particles oscillate with very small amplitudes. In the phase space, constructed by the distances between each particle and the side-wall, i.e., y_1/d and y_2/d , the attractor at this Reynolds number is a small limit cycle. The difference, s_l , between the maximum and minimum values of y_2/d of the limit cycle is defined as the size of the limit cycle. When $F=131.14$, the size is about 0.02. This periodic state is very close to the base steady state, therefore, the streamlines are almost stationary, as shown in Fig. 3. A flow circulation zone is produced as the cylinders rotate clockwise. The rotation of the leading cylinder seems to be rolling up the right wall. The trailing cylinder experiences a disturbed stream on its right side and rotates in the asymmetric flow on both sides. The rotations influence the staggered structure by inducing a Magnus effect on both cylinders. It is the Magnus effect that balances the wall repulsion and the interparticle repulsion, and maintains the nearly stable configuration.

When the value of the external force decreases from $F=131.41$, the size of the limit cycle decreases, as shown in Fig. 4. The results from simulations for $124 < F < 132$ show that the size of the limit cycles decrease rapidly as F decreases. The smallest size of the limit cycle obtained in the simulation is $s_l=0.007$ when $F=124.3$ and $Re=2.42$. These results, presented in Fig. 4, strongly suggest that a Hopf bifurcation occurs at around $F=124$.

IV. MULTIPLE STABLE STATES

In order to be able to compute solution branches that go through turning point transitions, the second type of initial condition which involves stepwise marching over a solution branch in small increments of Re (or F) is used. This is somewhat similar to branch tracing using continuation methods. Continuation of the solution on the primary (lower) periodic branch leads to a turning point at about $F=145$ (see Fig. 5). This leads to an unstable periodic branch (not shown

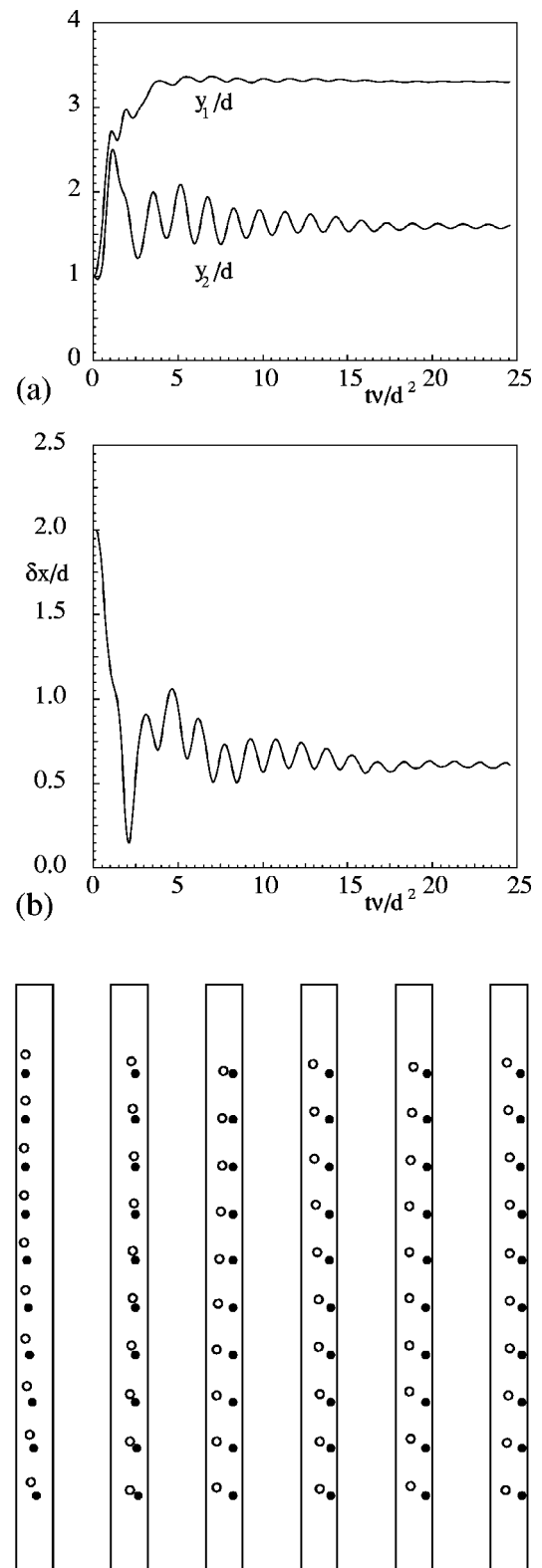


FIG. 2. Positions of the particles during sedimentation in a channel at Reynolds number $Re=2.539$ when $F=131.41$. Length and time are scaled by d and d^2/ν , respectively. (a) Horizontal position, (b) vertical distance, $\delta x = x_1 - x_2$, and (c) particle snapshots with a 0.1 time interval.

in Fig. 5), a second turning point at $F=135$, and a second stable periodic (upper) branch, as presented in Fig. 5. It is interesting to note that this simple particle sedimentation system has two stable states in the range of $135 < F < 145$. In

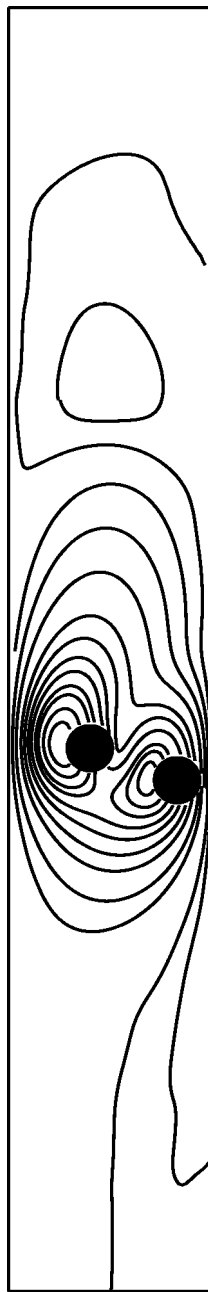


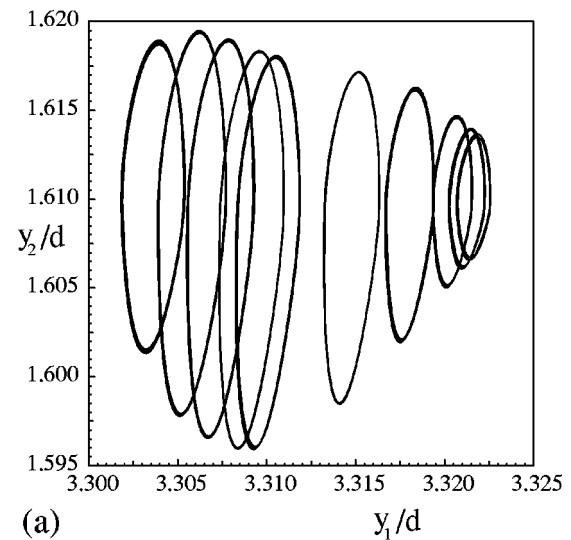
FIG. 3. Streamlines in the channel at Reynolds number $Re=2.539$ when $F=131.41$.

other words, in this range of the parameter the particles can follow two different trajectories as settling inside the channel.

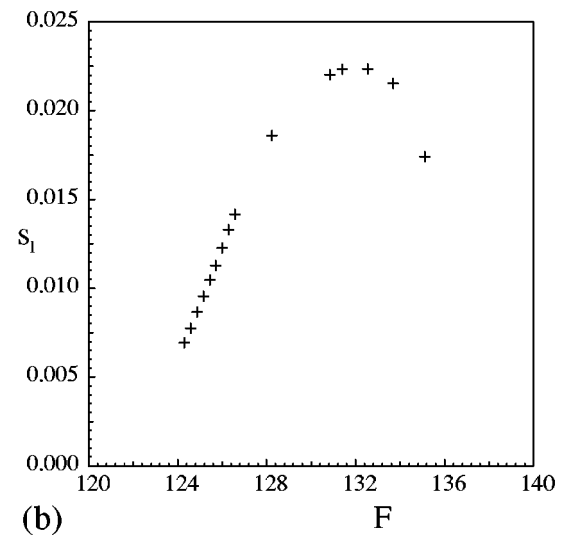
The limit cycles for several different values of external force between 125 and 143 are presented in Fig. 6. The three limit cycles labeled as 1, 2, and 3 are from the lower branch, while the other two, that is 4 and 5, are from the upper branch.

It is interesting to consider the dependence of the size of the limit cycle on the parameter, F , in order to explore any potential fundamental scaling characteristics.

For the lower branch, the centers of the limit cycles are located around $y_1/d \approx 3.3$ and $y_2/d \approx 1.6$. The relation be-



(a)



(b)

FIG. 4. (a) The limit cycles for Reynolds number around $Re=2.5$. The dimensionless external forces corresponding to these limit cycles, from right to left, are 124.30, 124.59, 125.16, 126.58, 128.24, 130.84, 131.41, 132.55, 133.69, and 135.11, respectively. (b) The size of the limit cycle vs the external force. A Hopf bifurcation is predicted at around $F=124$.

tween the Reynolds number and the external force on this branch is given by

$$Re = 0.027F - 1.011 \quad \text{if } 120 < F < 143.$$

The maximum size of the limit cycle in the lower branch is about $s=0.3$ at $F=142.8$. Further increasing the external force, the system falls inside the domain of attraction of the upper branch. A typical example of the attractor on the lower branch is shown by the cycle numbered 2 in Fig. 6, where the external force is $F=140.8$ and the corresponding Reynolds number is $Re=2.800$. The maximum and minimum values of y_2/d of this limit cycle are 1.690 and 1.536, respectively, and the size of the limit cycle is $s=0.154$.

For the upper branch, however, the centers of the limit cycles are around $y_1/d \approx 3.1$ and $y_2/d \approx 1.9$. The relation between the Reynolds number and the external force on this branch is given by

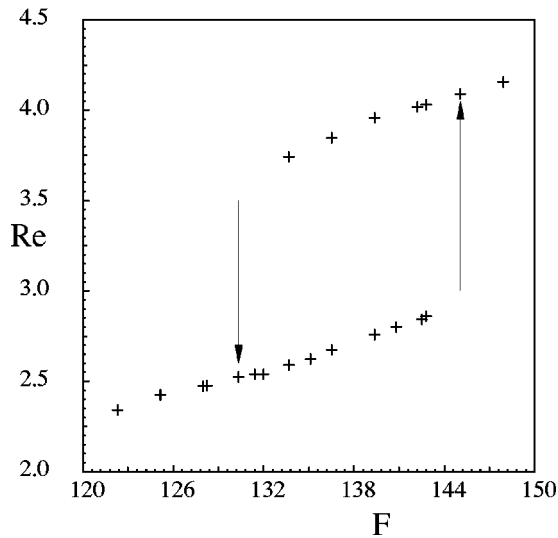


FIG. 5. The relation between external force and Reynolds number showing hysteresis between two coexisting attractors is found.

$$Re = 0.029F - 1.173 \quad \text{if } 133 < F < 150.$$

The minimum size of the limit cycle on the upper branch is about $s = 1.0$ when $F = 133$. Further decreasing the external force below 133, the system falls in the domain of attraction of the lower branch.

V. PERIOD-DOUBLING BIFURCATIONS

The upper periodic branch remains stable as F is increased up to about 153. For example, when $F = 147.91$ the Reynolds number is $Re = 4.216$. The attractor and the power spectrum density of $y_2(t)$ are shown in Figs. 7(a) and 7(b),

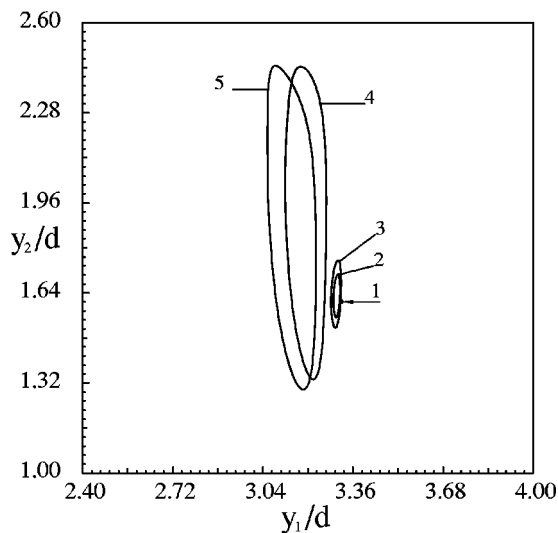
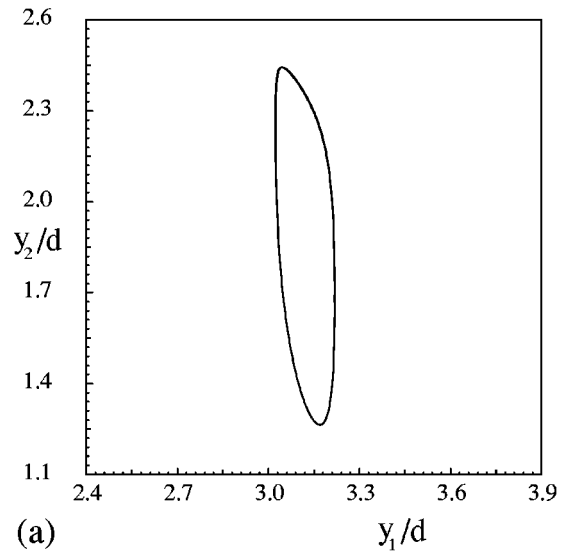
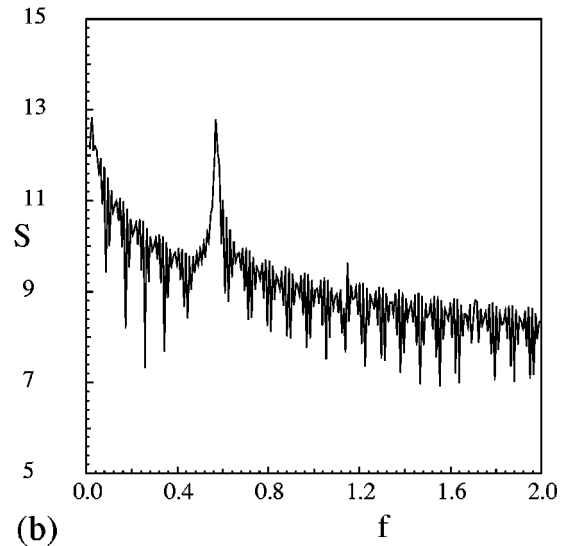


FIG. 6. The attractors in phase space. (1) $F = 125.16$, $Re = 2.426$; (2) $F = 140.80$, $Re = 2.800$; (3) $F = 142.79$, $Re = 2.861$; (4) $F = 133.79$, $Re = 3.742$; (5) $F = 142.79$, $Re = 3.988$. The first three attractors belong to the “lower periodic branch” while the last two belong to the “upper periodic branch.”



(a)

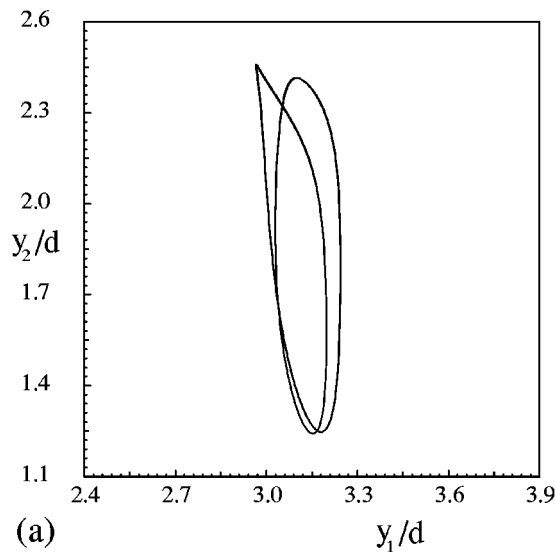


(b)

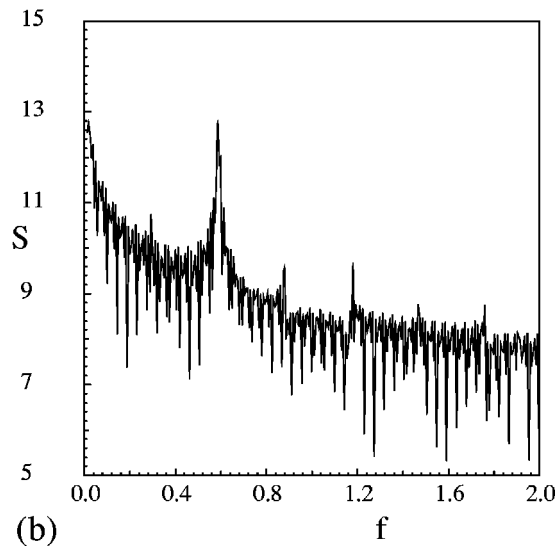
FIG. 7. (a) Trajectory of the circular cylinders in phase space, expanded by horizontal positions of two particles. External force is $F = 147.91$ and final Reynolds number is $Re = 4.216$. The equilibrium state is represented by a stable limit cycle. (b) Power spectrum density of signal $y_2(t)$ at $Re = 4.216$. The largest peak is at $f = 0.565$, related to the fundamental time period of the limit cycle.

respectively. The peak in the power spectrum is at $f = 0.565$, representing the fundamental frequency of the system. The period, T , of the oscillation, is $T = 1/f = 1.77$ (recall time is scaled by d^2/ν).

Further increasing the external force to $F = 156.44$, corresponding to $Re = 4.320$, the particle trajectory in the phase space shown in Fig. 8(a), and its power spectrum density in Fig. 8(b) show a different behavior. The largest peak at $f = 0.588$ is close to the base state frequency, while the next largest peak at $0.5f = 0.294$. Further analysis shows that at about $F = 153$, corresponding to $Re = 4.284$, the upper periodic branch (period-1 branch) undergoes period-doubling bifurcation, that is a sudden qualitative transition to a new equilibrium state (period-2).



(a)



(b)

FIG. 8. (a) Period-2 orbit of the circular cylinders in phase space. External force is $F = 156.44$ and the final Reynolds number is $Re = 4.320$. (b) Power spectrum density of signal $y_2(t)$ at $Re = 4.320$. The largest peak is at $f = 0.588$, related to the fundamental frequency of the base state, while the other peaks at $f/2 = 0.294$ and $3f/2 = 0.882$ are related to the period doubled state of the system.

The transition from period-1 to period-2 takes place at about $Re = 4.284$. In order to gain insight into the physics of this transition, the attractors at $Re = 4.284$ and $Re = 4.285$ are compared in Fig. 9 to construct and examine the characteristics of the destabilizing disturbance mode. The trajectory at $Re = 4.284$, before the transition, is a period-1 limit cycle, where at $Re = 4.285$, the trajectory is a period-2 limit cycle. The deviation of the trajectory of the leading particle between period-1 and period-2 states is much larger than the deviation in the trajectory of the trailing particle. Relative to the period-1 limit cycle at $Re = 4.284$, the first (second) half of the period-2 limit cycle at $Re = 4.285$ shifts slightly to the left (right). The snapshots of the particle configurations are shown in Fig. 10. The periods of the motion before and after

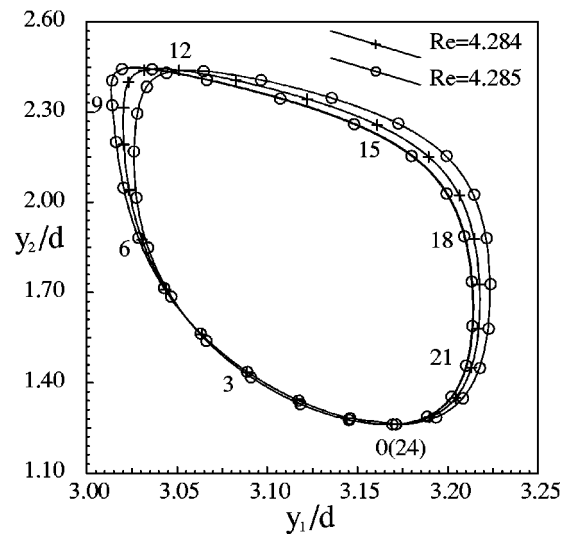


FIG. 9. The comparison between the limit cycles before and after the bifurcation. The numbers show the equal time intervals in the period-1 limit cycle. Notice that the scale at abscissa is different from Figs. 7(a) and 8(a), in order to make visible the two almost overlapped orbits.

the bifurcation are $T_1 = 1.755$ and $T_2 = 3.507 \approx 2T_1$, respectively.

In order to examine the physics of the transition, we examine the net and accumulated force on the particle through various segments of the trajectory in one period. Let us define t_0 such that at $t = t_0$ the trailing particle is at its leftmost position (i.e., maximum y_2) in the cycle. Dividing the period T_1 into 24 equal time increments, the snapshots at the end point of every time increment are shown in Fig. 10(a). The number in Fig. 10(a), n , corresponding to each snapshot, is related to time such that $n = 24(t - t_0)/T_1$. Similarly, the period-2 limit cycle is divided into 48 equal segments, where $n = 48(t - t_0)/T_2 \approx 48(t - t_0)/2T_1$ represents the numbered snapshots in Fig. 10(b). The difference between T_2 and $2T_1$ is very small, that is negligible. For period-2 limit cycle, numbers from 0 to 24 are for the first half cycle and numbers from 25 to 48 (same as position 0) are for the second half of the cycle. Since the limit cycle with these two Reynolds numbers are very close to each other, the corresponding snapshots for the two limit cycles almost coincide. For example, the configuration at snapshots 3 and 27 in the period-2 orbit is very close to the snapshot 3 in the period-1 orbit.

The horizontal component of the force (scaled by $d/\rho_f \nu^2$) on the leading particle, $F_1(Re, t)$ and $F_2(Re, t)$, are calculated at $Re = 4.284$ and $Re = 4.285$, respectively, and, their difference, $\delta f(t) = F_2(4.285, t) - F_1(4.284, t)$, as well as the accumulated quantity, $I(t) = \int_{t_0}^t \delta f(t) dt$, are computed and presented in Fig. 11. The “net force” in the first half cycle, $I(T_1)$, is positive, driving the leading particle to the right. However, in the second half cycle the “net force” on the leading particle, $I(2T_1) - I(T_1)$, is negative, driving the leading particle to the left. From Fig. 11(a) it is clear that the positive and negative net forces are mainly the contribution during the time the trailing particle is closest to the right wall, and therefore, to the leading particle. It is clear from

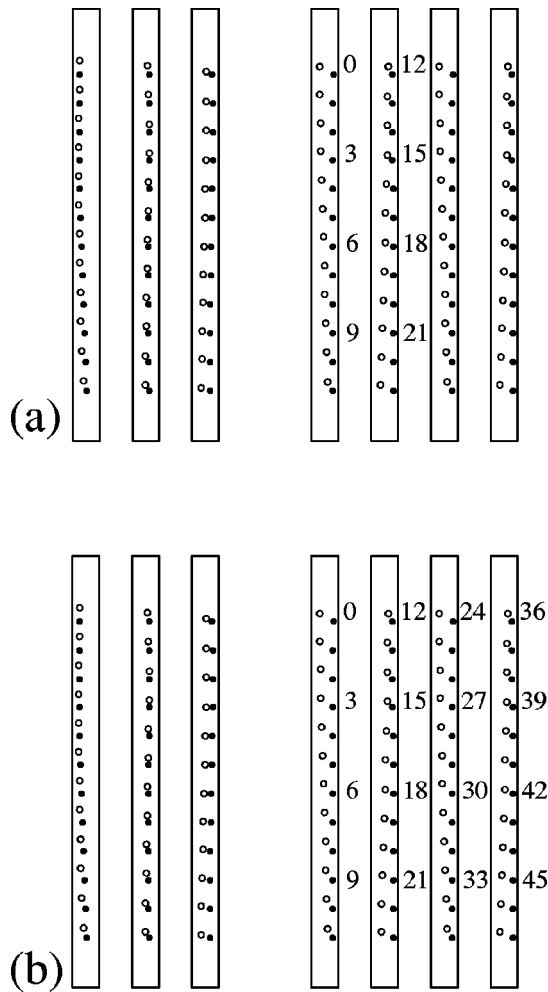


FIG. 10. The snapshots of the particles in period-1 and period-2 states. (a) $Re=4.284$, before the bifurcation; numbers by the third and fourth columns correspond to the numbers in Fig. 9. The time interval between two successive snapshots is 0.0732, or 1/24 of the period. The three left columns are the initial transient motion, and the four columns on the right-hand side are two complete periods at equilibrium state. (b) $Re=4.285$, after the bifurcation; the time interval between two successive snapshots is also 0.0732, or 1/24 of the period. The three left columns are the initial transient motion and the four columns on the right-hand side are a complete period at equilibrium state. The motion of the particles in both states appears identical because both are very close to the bifurcation point.

this analysis that the interaction of the two particles post-period-doubling bifurcation results in overshoot and then undershoot of the particle relative to their trajectory pre-bifurcation point.

Bifurcations to period-4 and period-8 attractors take place at $F=162.42$ ($Re=4.409$) and $F=163.50$ ($Re=4.431$), respectively. These limit cycles and power spectra for each are presented in Figs. 12 and 13. The faith of this system as Re (or F) increases is now predictable. This form of period-doubling bifurcation continues to occur at decreasing and eventually infinitesimally small increments of the relevant parameter at the onset of a low-dimensional chaotic state.

VI. THE CHAOTIC DYNAMICS

As Reynolds number increases further, the motion becomes more complex and non-periodic. At Reynolds number

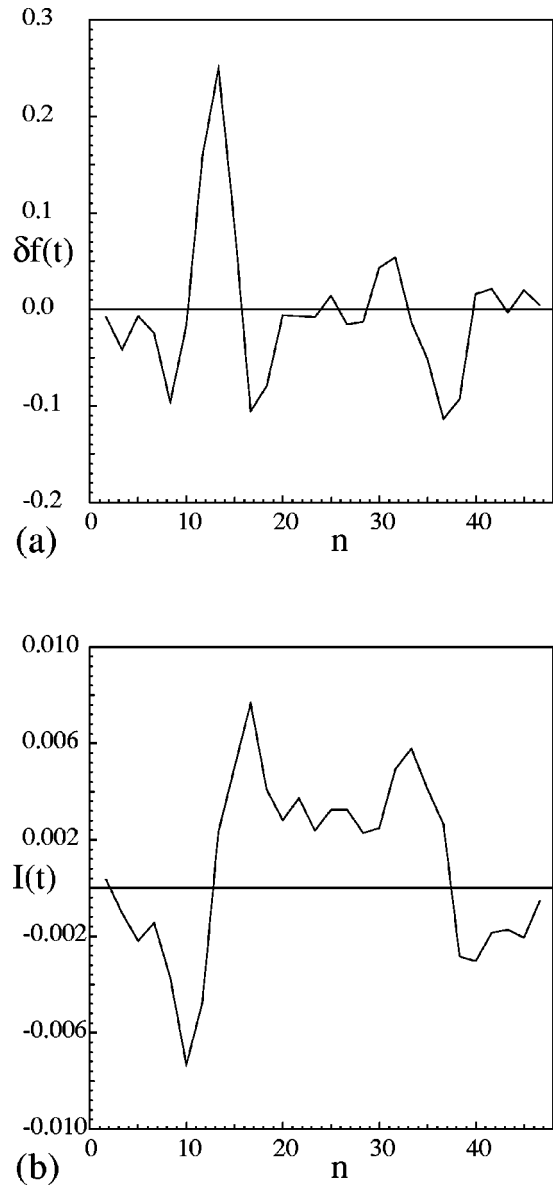
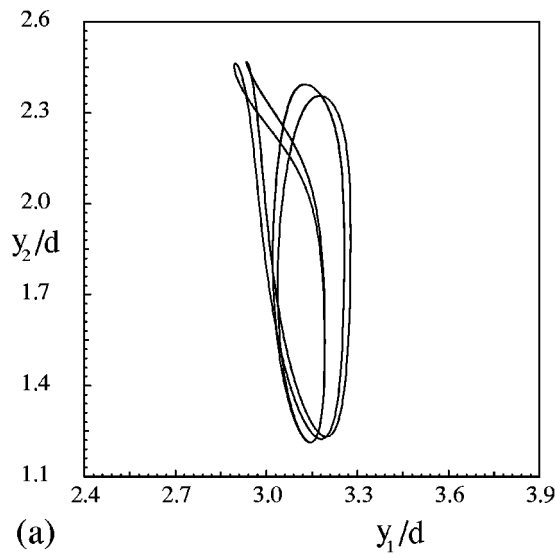


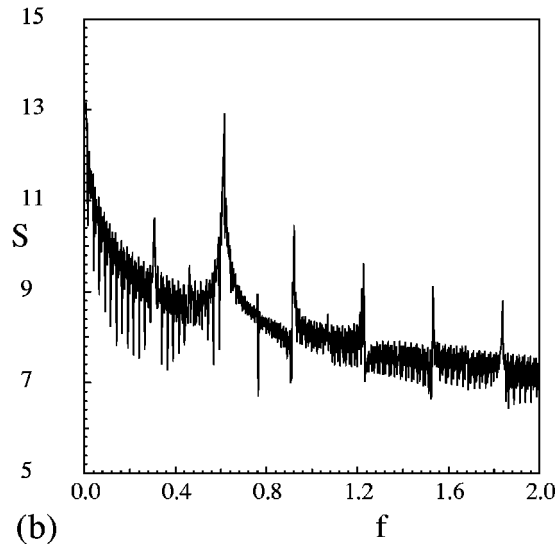
FIG. 11. The cross-stream component of the force on the leading particle where n is proportional to time (see the text and Fig. 10). (a) The net force, $\delta f(t)$, varies with time. (b) The integrate of net force, $I(t)$, is positive in the first half cycle, and negative in the second half cycle.

$Re=5.181$, the trajectory in the phase space and its power spectrum density, shown in Fig. 14(a), suggest existence of a chaotic attractor. The power spectrum density for this attractor is shown in Fig. 14(b). The broadband noise is typical of a low-dimensional chaotic motion of the system.

To better characterize the attractor, a return map is generated at section AB , identified in Fig. 14(a). The two end points A and B are defined by $(y_1/d, y_2/d) = (0.94625, 1.67825)$ and $(y_1/d, y_2/d) = (1.90625, 1.67825)$, respectively. As long as the trajectory intersects the section from below, the value of y_1/d is recorded in the return map. A series of signals, $y_1^{(n)}/d$ with $n=1, 2, \dots$, are then obtained. By this series of signals a return map can be constructed by successive intersections of projected flow with the segment AB . The result is a one-dimensional bimodal map, as shown in Fig. 15. The narrow bandwidth of the

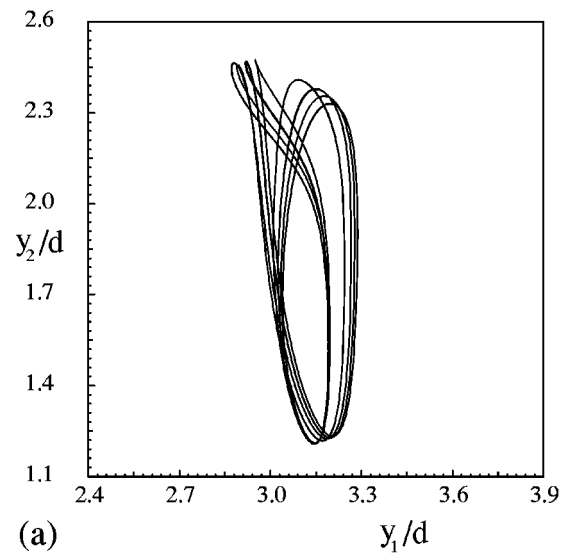


(a)

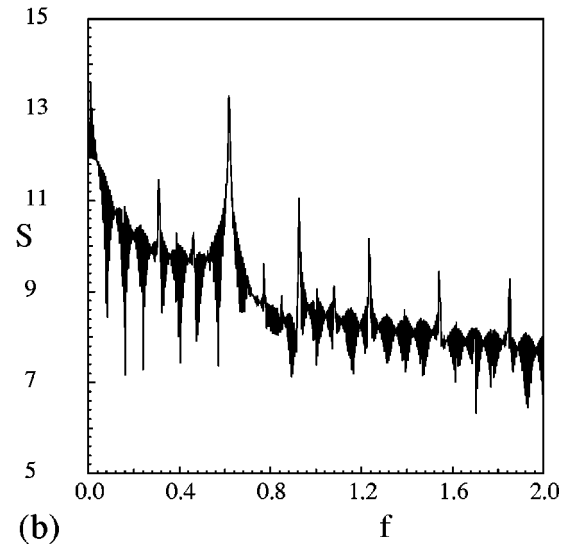


(b)

FIG. 12. (a) Period-4 orbit of the circular cylinders in phase space. The external force is $F = 162.42$ and the final Reynolds number is $Re = 4.409$. (b) Power spectrum density of signal $y_2(t)$ at $Re = 4.409$. The highest sharp peak is at $f = 0.616$, related to the basic frequency, while the lower peaks at $f/2 = 0.308$ and $3f/4 = 0.462$ are related to the doubled period of motion.



(a)



(b)

FIG. 13. (a) Period-8 orbit of the circular cylinders in phase space. The external force is $F = 163.50$ and the final Reynolds number is $Re = 4.431$. (b) Power spectrum density of signal $y_2(t)$ at $Re = 4.431$. The highest sharp peak is at $f = 0.6188$, related to the basic frequency, while the lower peaks at $f/2 = 0.3094$, $3f/4 = 0.4641$, and $5f/8 = 0.3868$ are related to the doubled period of motion.

map demonstrates a low-dimensional chaotic attractor. Unlike typical sub-harmonic bifurcations to chaotic state showing a unimodal return map, this case shows a more complex bimodal map where the correlation dimension must be computed numerically.

The correlation dimension of the strange attractor is calculated by taking the single scalar function $y_1(t)$ of the system state and reconstructing the dynamics in an m -dimensional space using the delay-coordinate technique.²³⁻²⁵ Denoting m -dimensional vector

$$\mathbf{X}_j = (y_1(t_j), y_1(t_{j+1}), \dots, y_1(t_{j+m-1})),$$

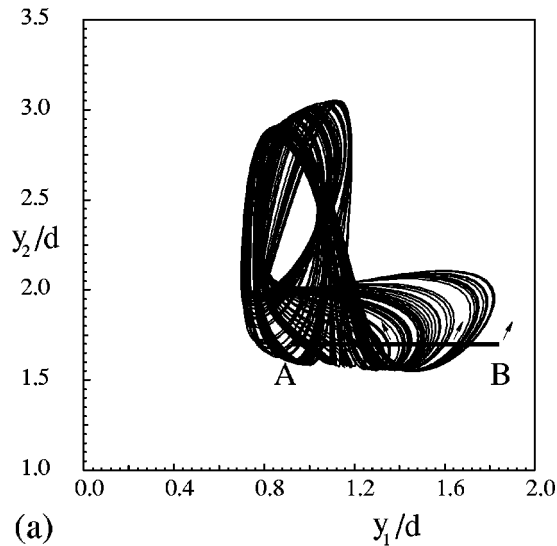
where $t_j = t_0 + j\Delta t$, the distance between two vectors \mathbf{X}_i and \mathbf{X}_j is defined by

$$|\mathbf{X}_i - \mathbf{X}_j| = \max_{0 \leq k < m} |y_1(t_{i+k}) - y_1(t_{j+k})|.$$

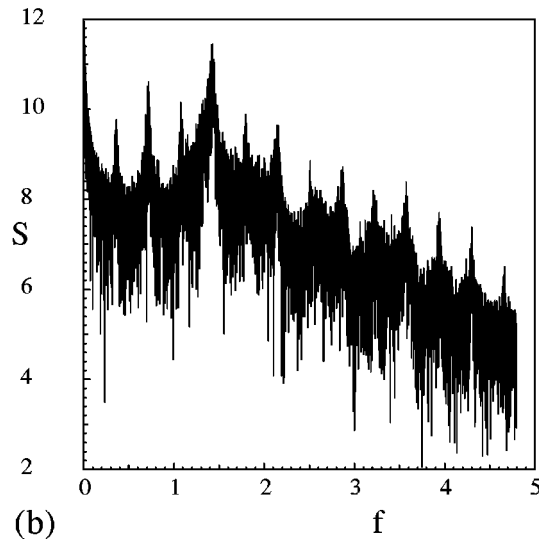
Assuming that there are a total number N of vectors \mathbf{X}_j in the m -dimensional space, the total number of pairs of vectors with distance less than δ is

$$N_\delta = \sum_{j=1}^N \sum_{i=j+1}^N \Theta(\delta - |\mathbf{X}_i - \mathbf{X}_j|),$$

where $\Theta(x)$ is the Heaviside step function defined as $\Theta(x) = 0$ for $x \leq 0$ and $\Theta(x) = 1$ for $x > 0$. By measuring the slope of $\log N_\delta$ vs $\log \delta$ when N is large enough, presented in Fig. 16, the correlation dimension $D_2 \approx 2$ is obtained. The correlation dimension provides fundamental characterization of a strange attractor. The time series of the m -dimensional vector, \mathbf{X}_j , reflects the nature of the chaotic behavior of the system. The correlation dimension $D_2 \approx 2$ here implies that by using a three(or higher)-dimensional space with coordi-



(a)



(b)

FIG. 14. (a) Trajectory of the circular cylinders in phase space. Final Reynolds number is $Re=5.181$. The complex motion suggests the existence of a strange attractor. The heavy solid line is the location of the section where a return map is generated. (b) Power spectrum density of signal $y_2(t)$ at $Re=5.181$. The broadband noise spectrum is due to the chaotic nature of motion.

notes $(y_1(t+j\Delta t), y_1(t+(j+1)\Delta t), y_1(t+(j+2)\Delta t))$ to represent the time series, the set of solution points will reside in a two-dimensional space.

VII. SUMMARY AND CONCLUSIONS

The structure of various attractors representing the hydrodynamic system is summarized in Fig. 17. When $Re=2.56$, the particle trajectories are such that the leading particle is always on the right side of the trailing particle ($y_2 < y_1$). As Reynolds number increases, the position of the attractors moves to a location with smaller y_1 and larger y_2 ($y_2 > y_1$). That is, the leading particle moves further away from the right wall, while the trailing particle moves closer to the right wall. At about $Re=4.5$, the two particles exchange their final position, with the leading particle settling on the left of the channel while the trailing particle follows

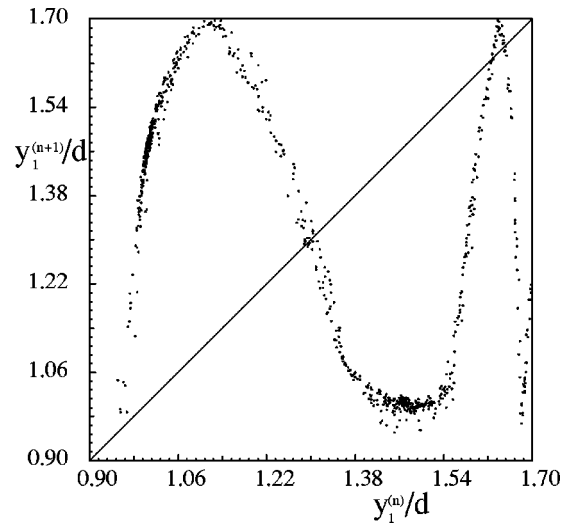


FIG. 15. Return map constructed by successive intersections of projected flow with section, identified in Fig. 14(a). The return map is bimodal.

on the right side. Obviously, the chaotic attractor, represented in Fig. 17, has a mirror image on the other quadrant of the phase space by simply exchanging the two particles (i.e., $y'_1=y_2$ and $y'_2=y_1$).

It has been known from previous studies that the interaction of two solid circular cylinders settling in a two-dimensional vertical channel results in qualitatively different settling behavior as Re varies.^{8,15} The results presented in this work show that the steady state at low Re becomes unstable at a critical Re giving rise to a Hopf bifurcation and being replaced by a time periodic state. As Re increases, the first periodic branch undergoes a turning point leading to an unstable branch with a second turning point giving rise to a second stable periodic branch. Further increasing the Reynolds number, the second stable periodic (upper) branch goes through period-doubling bifurcations. A cascade of period-

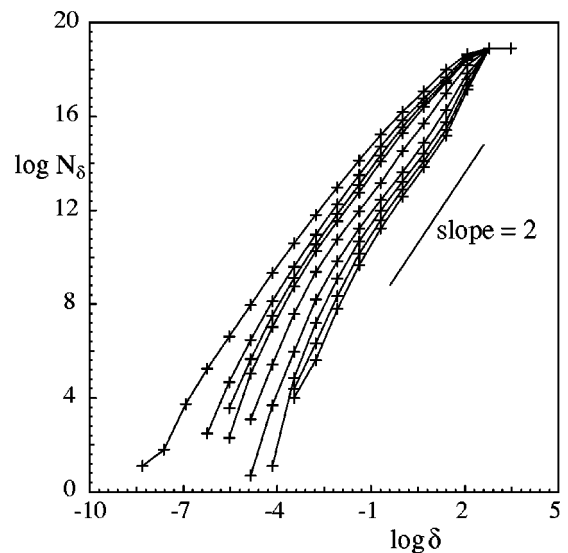


FIG. 16. Calculation of the correlation dimension D_2 of the strange attractor. The embedding dimension used for the present calculation is, from left to right, 2, 3, 4, 5, 10, 20, 30, 40, and 50, respectively.

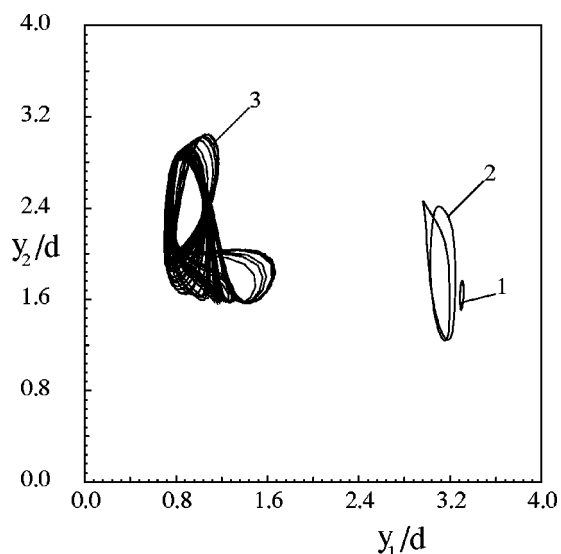


FIG. 17. The location of the orbits of the circular cylinders in phase space. (1) Damped oscillations (lower attractors in hysteresis are also in this region); (2) period-doubling bifurcations (higher attractors in hysteresis are also in this region); (3) chaotic motion.

doubling bifurcations occurs leading the system to a low dimensional chaotic state characterized by a strange attractor.

The high level of numerical accuracy provided by the ALD' lattice-Boltzmann method²² has made it possible to compute the particle trajectories over long time periods, and consequently to find the precise nature of the system's dynamics.

ACKNOWLEDGMENTS

This paper was originally presented at the Symposium on Multi-Component and Multiphase Fluid Dynamics, in conjunction with the 14th U.S. National Congress of Applied Mechanics. The Symposium celebrated the pioneering contributions in fluid mechanics by Daniel D. Joseph. We acknowledge helpful discussions with Dr. M. Ding. This work has been supported in part by the National Science Foundation (CTS-0130326).

¹J. F. Brady and G. Bossis, "The rheology of concentrated suspension of spheres in simple shear flow by numerical simulation," *J. Fluid Mech.* **155**, 105 (1985).

²S. Kim and S. J. Karrila, *Microhydrodynamics: Principles and Selected Applications* (Butterworth-Heinemann, Boston, 1991).

³L. M. Hocking, "The behaviour of clusters of spheres falling in a viscous fluid, Part 2, slow motion theory," *J. Fluid Mech.* **20**, 129 (1964).

⁴E. Wacholder and N. F. Sather, "The hydrodynamic interaction of two unequal spheres moving under gravity through quiescent viscous fluid," *J. Fluid Mech.* **65**, 417 (1974).

⁵H. Brenner, "Hydrodynamic resistance of particles at small Reynolds numbers," *Adv. Chem. Eng.* **6**, 287 (1966).

⁶G. K. Batchlor, "Transport properties of two-phase materials with random structure," *Annu. Rev. Fluid Mech.* **6**, 227 (1974).

⁷L. G. Leal, "Particle motion in a viscous fluid," *Annu. Rev. Fluid Mech.* **12**, 435 (1980).

⁸H. H. Hu, D. D. Joseph, and M. J. Crochet, "Direct simulation of fluid particle motions," *Theor. Comput. Fluid Dyn.* **3**, 285 (1992).

⁹O. G. Harlen, R. R. Sundararajakumar, and D. L. Koch, "Numerical simulations of a sphere setting through a suspension of neutrally buoyant fibres," *J. Fluid Mech.* **388**, 355 (1999).

¹⁰T. W. Pan, D. D. Joseph, and R. Glowinski, "Modelling Rayleigh-Taylor instability of a sedimenting suspension of several thousand circular particles in a direct numerical simulation," *J. Fluid Mech.* **434**, 23 (2001).

¹¹R. Zenit, D. L. Koch, and A. S. Sangani, "Measurements of the average properties of a suspension of bubbles rising in a vertical channel," *J. Fluid Mech.* **429**, 307 (2001).

¹²A. F. Fortes, D. D. Joseph, and T. S. Lundgren, "Nonlinear mechanics of fluidization of beds of spherical particles," *J. Fluid Mech.* **177**, 467 (1987).

¹³D. D. Joseph and D. Ocampo, "Slip velocity and lift," *J. Fluid Mech.* **454**, 263 (2002).

¹⁴N. A. Patankar, P. Y. Huang, T. Ko, and D. D. Joseph, "Lift-off of a single particle in Newtonian and viscoelastic fluids by direct numerical simulation," *J. Fluid Mech.* **438**, 67 (2001).

¹⁵J. Feng, H. H. Hu, and D. D. Joseph, "Direct simulation of initial value problems for the motion of solid bodies in a Newtonian fluid, Part 1, Sedimentation," *J. Fluid Mech.* **261**, 95 (1994).

¹⁶A. J. C. Ladd, "Numerical simulations of particulate suspensions via a discretized Boltzmann equation, Part 1, Theoretical foundation," *J. Fluid Mech.* **271**, 285 (1994).

¹⁷A. J. C. Ladd, "Numerical simulations of particulate suspensions via a discretized Boltzmann equation, Part 2, Numerical results," *J. Fluid Mech.* **271**, 311 (1994).

¹⁸C. K. Aidun and Y. Lu, "Lattice-Boltzmann simulation of solid particles suspended in fluid," *J. Stat. Phys.* **81**, 49 (1995).

¹⁹C. K. Aidun, Y. Lu, and E. Ding, "Dynamic simulation of particles suspended in fluid, The 1997 ASME Fluids Engineering Division Summer Meeting," (FEDSM'97), 22-26 June 1997.

²⁰C. K. Aidun, Y. Lu, and E. Ding, "Direct analysis of particulate suspensions with inertia using the discrete Boltzmann equation," *J. Fluid Mech.* **373**, 287 (1998).

²¹E. Ding and C. K. Aidun, "The dynamics and scaling law for particles suspended in shear flow with inertia," *J. Fluid Mech.* **423**, 317 (2000).

²²E. Ding and C. K. Aidun, "Extension of the Lattice-Boltzmann method for direct simulation of suspended particles near contact," *J. Stat. Phys.* **112**, 685 (2003).

²³P. Grassberger and I. Procaccia, "Measuring the strangeness of strange attractors," *Physica A* **9**, 189 (1983).

²⁴M. Ding, C. Grebogi, E. Ott, T. Sauer, and J. A. Yorke, "Estimating correlation dimension from a chaotic time series: When does plateau onset occur?" *Physica D* **69**, 404 (1993).

²⁵M. Ding and W. Yang, "Deterministic point processes generated by threshold crossings: Dynamics reconstruction and chaos control," *Phys. Rev. E* **55**, 2397 (1997).